Crystal Structure at 1.45 Å Resolution of Alanine Racemase from a Pathogenic Bacterium, *Pseudomonas aeruginosa*, Contains Both Internal and External Aldimine Forms[†,‡]

Pierre LeMagueres,[§] Hookang Im,[§] Anna Dvorak,[§] Ulrich Strych,[§] Michael Benedik,[§] and Kurt L. Krause*[,§,||]

Department of Biology and Biochemistry, University of Houston, Houston, Texas 77204, and Section of Infectious Diseases, Department of Medicine, Baylor College of Medicine, Houston, Texas 77030

Received July 7, 2003; Revised Manuscript Received October 9, 2003

ABSTRACT: The structure of the catabolic alanine racemase, DadX, from the pathogenic bacterium *Pseudomonas aeruginosa*, reported here at 1.45 Å resolution, is a dimer in which each monomer is comprised of two domains, an eight-stranded α/β barrel containing the PLP cofactor and a second domain primarily composed of β-strands. The geometry of each domain is very similar to that of *Bacillus stearothermophilus* alanine racemase, but the rotation between domains differs by about 15°. This change does not alter the structure of the active site in which almost all residues superimpose well with a low rms difference of 0.86 Å. Unexpectedly, the active site of DadX contains a guest substrate that is located where acetate and propionate have been observed in the *Bacillus* structures. It is modeled as D-lysine and oriented such that its terminal NZ atom makes a covalent bond with C4′ of PLP. Since the internal aldimine bond between the protein lysine, Lys33, and C4′ of PLP is also unambiguously observed, there appears to be an equilibrium between both internally and externally reacted forms. The PLP cofactor adopts two partially occupied conformational states that resemble previously reported internal and external aldimine complexes.

Pseudomonas aeruginosa is an important Gram-negative pathogen that is capable of causing a wide variety of serious infections in humans including pneumonia, septicemia, endocarditis, and osteomyelitis (*1*). It is one of the top five causes of nosocomial infections, including infections in intensive care units (*2*). Patients with cystic fibrosis have a high incidence of often life-threatening *Pseudomonas* infections (*3*). The tenacious pathogenicity of *P. aeruginosa* is often coupled with high levels of antibiotic resistance. In fact, hospital isolates of *Pseudomonas* that are resistant to all commonly used antibiotics have been reported (*4*, *5*). As a result, it would be of significant public health importance to identify new leads for antibiotics directed at this organism.

Alanine racemase (EC 5.1.1.1) is an essential enzyme in prokaryotes. It is a pyridoxal 5′-phosphate (PLP)-containing[1] enzyme that catalyzes the interconversion of L-alanine and D-alanine, an essential building block in the biosynthesis of the peptidoglycan layer in cell walls. *Pseudomonas* contains two different homologous genes for alanine racemase (*6*). In *Salmonella typhimurium*, the *alr* gene is expressed constitutively at low levels to allow the biosynthesis of D-alanine (*7*) while, in *Escherichia coli*, the *dadX* gene is induced when cells are grown on L-alanine (*8*). Because alanine racemase is absent in virtually all eukaryotes, it has often been proposed as an ideal drug target for the development of new antibiotics (*9*, *10*).

Prior to the current era of structure-aided drug design, alanine racemase was the focus of research showing that many structural analogues of D-alanine inhibit the enzyme (*11*−*14*). Unfortunately, these inhibitors all suffered from a lack of specificity, thought to be in part because they acted on other PLP-containing enzymes, including those found in humans (*15*, *16*). One of these compounds, D-cycloserine (DCS), was developed commercially. It acted by inhibiting alanine racemase, as well as the functionally related enzyme, D-ala ligase. DCS is still the only currently marketed antibiotic whose action is based on alanine racemase inhibition. However, its clinical use is limited because of severe side effects, which include central nervous system toxicity (*17*−*19*).

Since 1997, several studies on the alanine racemase from *Bacillus stearothermophilus* have elucidated important aspects of the enzyme's tertiary structure and essential features of how the enzyme binds substrate and carries out catalysis. Ringe et al. reported the crystal structure of the alanine racemase enzyme Alr from *B. stearothermophilus* with acetate and propionate (*20*, *21*) and a form with a covalently bound inhibitor, the alanine analogue alanine phosphonate (*22*). These studies confirmed that this enzyme is a homodimer, with each of the monomers containing two domains. The N-terminal domain is an α/β barrel, within which the pyridoxal 5′-phosphate is bound to the protein via an

[†] This publication was supported, in part, by grants from the National Institutes of Health (AI-46340), the W. M. Keck Foundation, and the Robert A. Welch Foundation.

[‡] The coordinates have been deposited in the Protein Data Bank with the entry code 1RCQ.

* To whom correspondence should be addressed. Tel: (713) 743-8370. Fax: (713) 743-8370. E-mail: kkrause@uh.edu.

[§] University of Houston.

[||] Baylor College of Medicine.

[1] Abbreviations: HEPES, *N*-2-hydroxyethylpiperazine-*N*′-2-ethanesulfonic acid; MAD, multiwavelength anomalous dispersion; DCS, D-cycloserine; PLP, pyridoxal 5′-phosphate; rms, root-mean-square.

10.1021/bi030165v CCC: $25.00
Published on Web 11/25/2003

Table 1: Data Collection and Processing Statistics

	MAD 1	MAD 2	MAD 3	MAD 4	native
λ (Å)	0.9795	0.9791	0.9611	0.9840	0.9840
resolution (Å) (last shell)		2.00 (2.07−2.0)			1.45 (1.48−1.45)
mosaicity		0.23			0.40
observations	144192	145322	151173	143764	359534
unique reflections	25234	25416	25671	25309	56981
R-merge[a] (%)	3.7 (6.6)	7.5 (13.7)	5.1 (10.2)	3.1 (7.9)	3.0 (18.6)
completeness (%)	96.5 (79.5)	96.9 (79.3)	97.9 (86.1)	96.5 (78.8)	84.7 (36.2)
$\langle I/\sigma \rangle$	35.0 (15.9)	22.0 (8.7)	27.2 (11.7)	33.8 (8.6)	51.5 (3.9)

[a] *R*-merge $= \sum|I_{obs} - I_{avg}|/\sum|I_{avg}|$.

aldimine linkage to Lys39. The C-terminal domain interacts with the TIM barrel of the opposite monomer to complete the dimer. According to these structural reports, the architecture of the alanine racemase from *B. stearothermophilus* possesses a unique fold among PLP-containing enzymes in the structural classification proposed by Jansonius (*23*). Recent theoretical (*24*) and experimental (*25*) studies on the complex of Alr with its natural substrate (L-alanine) and PLP cofactor are consistent with the involvement of Lys39, Arg136, Arg219, and Tyr265′ (265′ from the second monomer) in the catalytic cycle of Alr. Structural studies of the complex formed between alanine racemase and DCS have also been completed and indicate stable, covalent adduct forms between PLP and this antibiotic (*26*), consistent with earlier reports on other PLP enzymes (*27*, *28*).

Structures of alanine racemase from pathogenic bacteria could, in principle, serve as a template for the design of alanine racemase inhibitors of greater specificity and less toxicity to humans. There is, however, some doubt within the drug-design community concerning the size of the active site pocket of alanine racemase and whether it contains sufficient volume to support an antimicrobial design effort. There is concern that the active site will not allow for the design of agents that would not also inhibit eukaryotic PLP-containing enzymes. In addition, it is unknown if there will be sufficient intraspecies variability to allow for the design of species specific inhibitors. Finally, even the very basic question of whether alanine racemase is always dimeric is being debated (*20*, *29*).

To help address some of these issues, we report here the 1.45 Å resolution structure of the catabolic alanine racemase, DadX, from *P. aeruginosa* (*6*). DadX is a dimeric enzyme composed of two identical 357 residue monomers. Its sequence possesses 28% identity to the *B. stearothermophilus* alanine racemase. Its K_M for substrate is 1.4 mM, while its V_{max} for racemization is about 145 U/mg, all values close to that of related enzymes from other bacteria (*6*).

This alanine racemase structure is the first from an important human pathogen and allows for a detailed comparison to earlier structures from *Bacillus*. While the structures are very similar in both secondary and tertiary features, we do report significant differences between them including altered tertiary packing and some variation in secondary structure. The resolution of this structure allows us to describe a few structural features of possible mechanistic importance. We report some evidence for a nonprotonated state of the PLP pyridine nitrogen. We also report the unexpected presence of a guest compound within the active site and describe evidence for its involvement in a partially occupied external aldimine formation with PLP.

MATERIALS AND METHODS

Purification. E. coli BL21 (DE3) containing the plasmid pMB1912 ($dadX_{PA}$) (*6*) was grown at 37 °C in Luria broth containing ampicillin (100 μg/mL). At $OD_{600} = 0.5$, IPTG (0.5 mM) was added, and cells were grown overnight at 30 °C. Cell pellets were resuspended in 50 mM Tris, pH = 7.6, 0.5 mM PLP, and 150 μg of purified *Serratia marcescens* nuclease was added. Cells were lysed using a Spectronic French Press at 16 000 psi, and cell debris was removed by centrifugation. $(NH_4)_2SO_4$ 20 and 60% cuts were done, and following the final cut, the protein pellet was dialyzed against 20 mM Tris, pH = 7.6 and filtered through a 0.45 μm syringe filter. This material was loaded on a Pharmacia Q-Sepharose HP column and eluted with a 0−0.5 M NaCl gradient. Pooled fractions were concentrated and loaded on a Pharmacia Superdex 200 column equilibrated with 20 mM Tris, pH = 7.6 and 400 mM NaCl. Fractions containing alanine racemase were pooled and concentrated. To produce selenomethionine modified protein, *E. coli* B834 (Novagen) was used as a host for pMB1912, and cells were grown in M9 medium supplemented with vitamins and selenomethionine. After harvest, cells were lysed using B-PER (Pierce) and purified as described previously.

Crystallization. The alanine racemase enzyme DadX (15 mg/mL) was crystallized at 4 °C in sitting drops equilibrated versus 1.5 M $(NH_4)_2SO_4$, 2% PEG400, and 0.1 M HEPES, pH = 7.5. Rectangular, deeply yellow crystals were obtained in space group $C222_1$ with unit cell parameters $a = 72.68$ Å, $b = 76.13$ Å, and $c = 136.27$ Å. There is one DadX monomer per asymmetric unit.

Data Collection and Processing. Multiple anomalous dispersion (MAD) data were collected at beamline 12-BMD of the BioCARS sector of the Advanced Photon Source at Argonne National Laboratory. Structure determination using MAD phasing was carried out to avoid any phase bias from molecular replacement. No molecular replacement solution was attempted. All data were collected at −180 °C using a Q4 ADSC CCD detector. Four data sets, each to a resolution of 2.0 Å, were collected on one crystal of selenomethionine DadX (0.2 × 0.2 × 0.1 mm). Native data were collected on a wild-type crystal (0.3 × 0.3 × 0.15 mm) to 1.45 Å resolution. The data were integrated, scaled, reduced, and merged using the HKL package (*30*). The data collection and data processing statistics for the MAD and native data sets are listed in Table 1.

Structure Determination and Refinement. Using the four MAD data sets, all nine selenium atomic positions were located using the program SOLVE (*31*), and the data were phased to 2.0 Å resolution with an overall mean figure of

merit of 84%. The protein was traced using ARP/wARP in mode *warpNtrace* (*32*−*34*). A total of 10 iterations, consisting of one cycle of model building and 10 cycles of positional and B_{iso} refinements using data up to 1.45 Å, yielded the entire trace of the protein, including both N- and C-termini. At the conclusion of the ARP/wARP run, the *R*-factor and R_{free} (calculated on 5% of the whole data set) were 17.7 and 23.4%, respectively, and the connectivity index measured by ARP/wARP was excellent at 98%.

Using the side-chains-docking script *side_dock.sh* of ARP/wARP, and the amino acid sequence (*6*), all side chains except Met1 and Ala357 were next fit into electron density. The N- and C-terminal residues and the PLP cofactor were then manually placed into density, and all solvent molecules remaining from ARP/wARP were removed. The protein model was submitted to positional and isotropic *B*-factor refinement using the program SHELXL (*35*) with standard restraints. Next, 306 water molecules were added by combining ARP/wARP in mode *solvent building* with SHELXL refinements. At this point, *R* and R_{free} were 20.1 and 24.1%, respectively, but because of the high resolution of the data (1.45 Å), we carried out anisotropic thermal parameter refinement for those protein atoms with a real space correlation coefficient higher than 0.90. Real space correlation coefficients between the model and the electron density map obtained with coefficients $2F_{obs} - F_{calc}$ (Sigma-A map) (*35*) were calculated using the program O (*36*). The average correlation for the entire monomer was 0.96. The 15 atoms of the PLP cofactor were also included in anisotropic refinement, but all solvent atoms were refined isotropically. Anisotropic refinement resulted in *R* and R_{free} parameters of 17.0 and 21.9%. Placement of hydrogen atoms and addition of a solvent mask both in SHELXL further decreased the *R* and R_{free} values to 14.9 and 20.6%, respectively.

Refinement of Extra Density. At this stage, $F_{obs} - F_{calc}$ difference Fourier maps (Sigma-D map) (*35*) revealed large contiguous electron density of up to 3.5σ adjacent to the PLP cofactor. We also noted a bulge in the $2F_{obs} - F_{calc}$ density of C4′ from PLP directed toward this contiguous density. We attempted to fit this extra density with small molecules found in our purification and crystallization solutions, including Tris, HEPES, acetate, and propionate, and all 20 amino acids. At the conclusion of these efforts, we found that the best geometrical fit was obtained with a molecule of D-lysine modeled into this density such that the terminal nitrogen atom NZ of the side chain forms an external aldimine linkage with the PLP ring (see also Results and Discussion and Figure 7). The coordinates of the putative D-lysine were then added into the protein model with restraints on the 1,2 and 1,3 distances identical to those used for common lysine residues in proteins. To more accurately model the presence of both internal and external aldimine complexes, additional refinement was performed as follows: (i) PLP was assumed to exist on two positions, each with an occupancy of 0.5; (ii) for each position, planarity restraints were imposed for the ring and its four substituting atoms (C2′, O3′, C4′, and C5′) and for the dihedral angle defined by C4′, C4, C3, and O3′; (iii) the distance between C4′ (both positions) and NZ (lysine residues) was restrained to 1.30 Å; (iv) D-lysine and PLP atoms were refined using isotropic temperature factors. After 40 cycles of refinement, *R* and R_{free} were refined to 14.8 and 20.6% for 49 538 reflections between 30 and 1.45 Å with $I > 2\sigma(I)$ (Table 2). The final DadX structure contains 357 residues, 2753 non-hydrogen protein atoms, 306 water molecules, 30 non-hydrogen PLP atoms with an occupancy of 0.5, and 10 non-hydrogen D-lysine atoms. The root-mean-square deviations from ideality for bond lengths and angles are 0.01 Å and 2.18°.

Table 2: Final Refinement Statistics for DadX

R-factor[a] (%)	14.8
R_{free} (for 2546 reflections, %)	20.6
average *B*-factors	
main chain[b] (Å^2)	19.1
side chain[c] (Å^2)	24.0
waters	31.0
rms deviations	
bond lengths (Å)	0.01
bond angles (deg)	2.18
no. of reflections > 2σ	49538
no. of residues (% protein)	357 (100%)
no. of protein atoms	2753
no. of PLP atoms[d]	30
no. of water molecules	306

[a] *R*-factor = $\sum|F_{obs} - F_{calc}|/\sum|F_{obs}|$. [b] Anisotropic model. [c] All but 21 side chains refined with anisotropic model. [d] Two PLPs with 0.5 occupancy included in model.

RESULTS AND DISCUSSION

Description of the Overall Structure. The structure of DadX is a dimer formed by a head-to-tail association of two monomers such that the N-terminal domain of one monomer interacts with the C-terminal domain of the second monomer. The monomers are symmetrically related by a crystallographic 2-fold axis (parallel to the unit cell *a* axis). The DadX monomer consists of two different domains (Figure 1a). The N-terminal domain, comprising residues 1−228, is an eight-stranded α/β barrel. The C-terminal domain includes residues 229−357 and is primarily composed of β-structure. The PLP cofactor is covalently linked to Lys33 and points toward the center of the α/β barrel. When viewed from the side, the two domains of the monomer are bent relative to each other at approximately a 130° angle (Figure 1b).

The amino acid sequence identity between DadX from *P. aeruginosa* and Alr from *B. stearothermophilus* (*20*) is 28% (Figure 2), and as expected, their tertiary folds are very similar (Figure 3). Interestingly, Figure 4 shows that only one domain of DadX can be superimposed on an Alr monomer at a time. This is due to a rotation of the C-terminal domain in the direction of the N-terminus in Alr that is not present in DadX. The rotation is approximately 15° around a pivot that would be perpendicular to the plane of Figure 4 and pass through the C_α of Gln342 (Glu355 in Alr). Comparison of the polar interactions at the monomer interface in DadX and Alr shows that the structural basis for this rotation is likely to arise from three separate hydrogen bonds that are missing from DadX but present in Alr. These three bonds involve Asp68 and Arg89 of the first Alr monomer and Phe4, His5, and Asn379 of the second Alr monomer. Residues corresponding to Phe4 and Asn379 are missing in DadX because the N- and C-terminal ends of DadX are shorter than Alr by four residues and 17 residues, respectively (Figure 2).

Despite the difference in the orientation of the monomer domains in DadX as compared to Alr, the geometry of the active site in both enzymes is maintained. In both, the

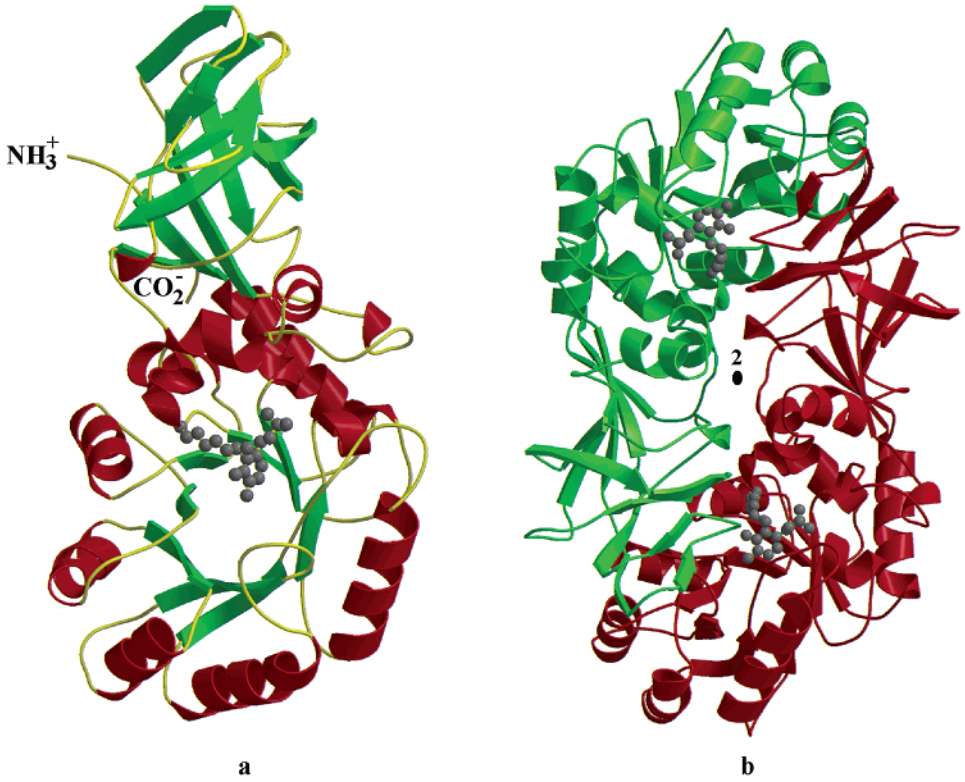

FIGURE 1: Ribbon diagram of (a) the monomer and (b) the dimer of the alanine racemase DadX from *P. aeruginosa*. The side chain of Lys33 and the PLP cofactor are represented as gray spheres. The symbol labeled 2 in panel b marks the position of the crystallographic 2-fold axis relating the two monomers.

```
Bst_alr   1    MNDFHRDTWAEVDLDAIYDNVENLRRLLPDDTHIMAVVKANAYGHGDVQVARTALEAGAS
Pao_DadX  1    ----MRPARALIDLQALRHNYRLAREATG--ARALAVIKADAYGHGAVRCAEALAAE-AD

Bst_alr  61    RLAVAFLDEALALREKGIEAPILVLGAS-RPADAALAAQQRIALTVFRSDWLEEASALYS
Pao_DadX 54    GFAVACIEEGLELREAGIRQPILLLEGFFEASELELIVAHDFWCVVHCAWQLEAIERAS-

Bst_alr  120   GPFPIHFHLKMDTGMGRLGVKDEEETKRIVALIERHPHFVLEGLYTHFATADEVNTDYFS
Pao_DadX 113   LARPLNVWLKMDSGMHRVGFFP-EDFRAAHERLRASGKVAKIVMMSHFSRADELDCPRTE

Bst_alr  180   YQYTRFLHMLEWLPSRPPLVHCANSAASLRFPDRTFNMVRFGIAMYGLAPSPGIKPLLPY
Pao_DadX 172   EQLAAFSAASQ-G-LEG-EISLRNSPAVLGWPKVPSDWVRPGILLYGATPFE-RA-HPLA

Bst_alr  240   -PLKEAFSLHSRLVHVKKLQPGEKVSYGATYTAQTEEWIGTIPIGYADGWLRRLQH-FHV
Pao_DadX 227   DRLRPVMTLESKVISVRDLPAGEPVGYGARYSTERRQRIGVVAMGYADGYPRHAADGTLV

Bst_alr  298   LVDGQKAPIVGRICMDQCMIRLPG-P-LPVGTKVTLIGRQGDEVISIDDVARHLETINYE
Pao_DadX 287   FIDGKPGRLVGRVSMDMLTVDLTDHPQAGLGSRVELWGP----NVPVGALAAQFGSIPYQ

Bst_alr  356   VPCTISYRVPRIFFRHKRIMEVRNAIGAGESSA
Pao_DadX 343   LLCNNK-RVPRVYSGA-----------------
```

FIGURE 2: Structure-based sequence alignment of *P. aeruginosa*, DadX, and *B. stearothermophilus* Alr. The sequences were aligned in QUANTA using a least-squares fit of the C_α atoms, and the alignment was adjusted manually upon examination of the superimposed structures.

interdomain rotation found in one monomer is compensated by the same phenomenon in the second monomer of the homodimer. Superposition of the complete monomer of DadX and Alr (PDB: 1SFT) results in an rms difference (C_α atoms) of 3.26 Å. However, superposition of the N- and C-terminal domains separately yields smaller rms differences (C_α atoms) of 1.88 and 1.63 Å, respectively (Figure 5).

N-Terminal Domain (Residues 1−*228).* Most of the structural differences between the N-terminal domains of DadX and Alr involve α-helices and loops located away from the dimer interface and arise from regions that are truncated or missing from DadX but present in Alr (Figure 2). In contrast, the regions near the active site (and thus, the dimer interface) superimpose very well. The average rms difference (C_α atoms) for these core residues from DadX and Alr is only 0.86 Å.

Residues located outside of the core of the α/*β* barrel of DadX and Alr show greater structural variation. For example,

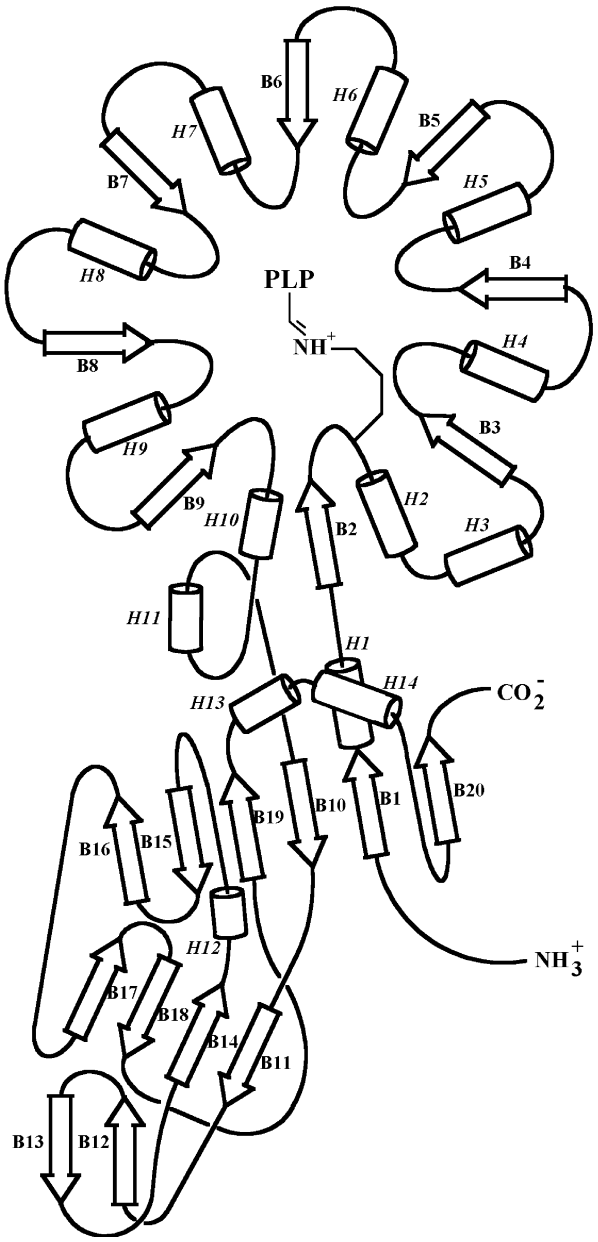

FIGURE 3: Topology diagram representing the secondary structure of DadX.

because the N-terminus of DadX is shorter than Alr by four residues (Figure 5a), the first residues that show satisfactory overlap are Ala6 of DadX and Ala10 of Alr. Because of insertions and deletions, most often in loop regions, there are several regions in Alr that do not superimpose well with DadX. For example, residues 18−27 in DadX superimpose poorly because DadX lacks residues that correspond to Asp30 and Asp31. The 219−227 region of DadX superimposes poorly due to a combination of deletion and insertion that alters the position of the α-helix H11 (Figure 5a). In addition, DadX shows significant structural differences near the following residues of Alr−Gly58, Ser119, Glu143, Leu192, Pro193, and Pro197. As noted, most of these residues do not directly interact with the second monomer or with residues within the active site, which may explain why the high variation in sequence is tolerated.

C-Terminal Domain (Residues 229−357). Ringe et al. have reported that the C-terminal domain of Alr has a unique topology (*20*). The fold of this domain is conserved with

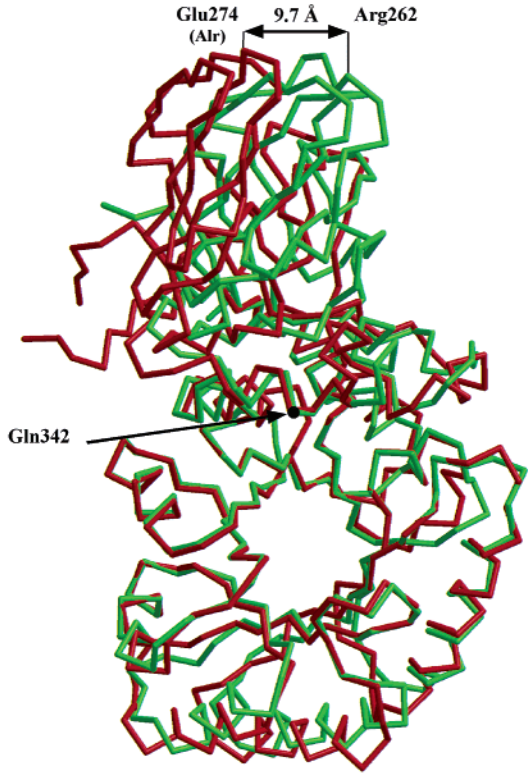

FIGURE 4: Superposition of the monomers of DadX (green) and Alr (red) obtained after a least-squares fit of the C_α atoms from the N-terminal domains exclusively. It reveals the different inter-domain rotations for DadX and Alr. At the top of the figure, the distance between structurally equivalent residues is reported.

minor differences in the DadX structure, as shown by the superposition in Figure 5b. In DadX, the C-terminal domain is composed of 12 β-strands and three α-helices. The first β-strand B1, although near the N-terminal domain, belongs to the C-terminal domain as it is inserted between B10 and B20 and participates in a six-stranded β-sheet (Figure 3). Two other β-sheets made of, respectively, four and two strands are also observed in this domain. All strands are antiparallel, except B20 and B1, which are parallel. The overall dimensions of the C-terminus domain are about 40 by 25 by 18 Å. Residues involved in the dimer interface superimpose best between DadX and Alr. For example, the rms difference for residues Tyr253, Ala273, and Asp302 represented in Figure 5b are 0.56, 0.68, and 0.32 Å, respectively.

Minor structural differences do exist in areas that do not interact with the second monomer upon dimerization. For example, in the turn between B18 and B19 of DadX (identified as loop 1 in Figure 5b), superposition is poor because this turn contains an insertion of two residues, Thr309 and Glu313. This loop ends up being wider and extends out of the protein by 4 Å more than in Alr. Further, in the turn between B19 and H13 of DadX, four residues of Alr are missing (i.e., Gln335, Gly336, Asp337, and Glu338), resulting in the loss of B17 and B18 (Alr labels) from DadX (identified as loop 2 in Figure 5b). This loop in Alr protrudes about 7 Å farther from the protein than in DadX. Finally, the C-terminus is 17 residues longer in Alr than DadX eliminating B20 of Alr (373−378) from the DadX structure. Note that the five-stranded β-sheet found in this domain in Alr is composed of six strands in DadX due to slight

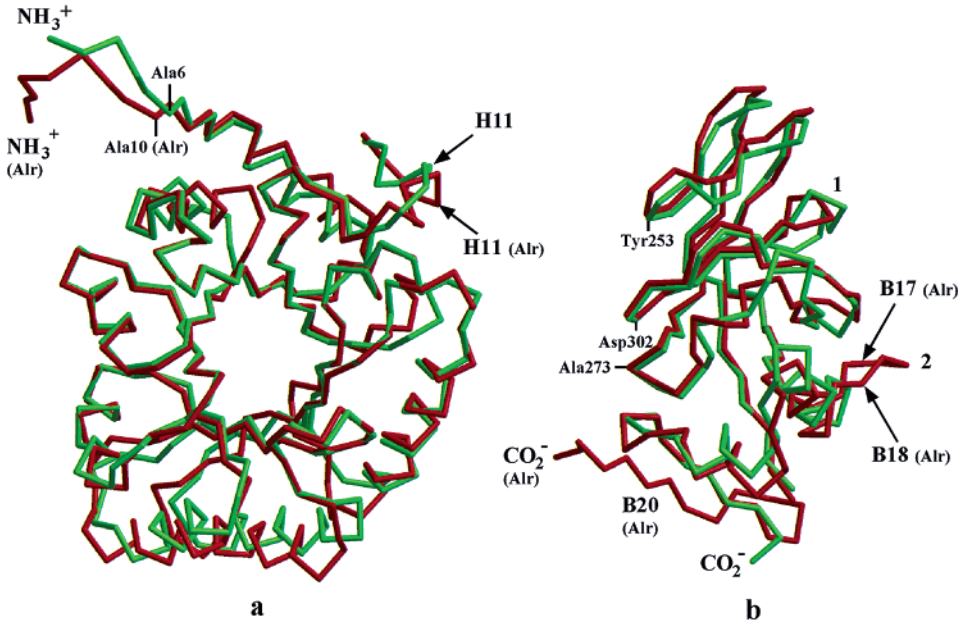

FIGURE 5: Superposition of DadX (green) and Alr (red) obtained after a least-squares fit of the C_α atoms of (a) the N-terminal domain and (b) the C-terminal domain. The labels refer to equivalent regions of DadX and Alr showing significant displacement (see text). Alr annotations refer to the *Bacillus* Alr structure.

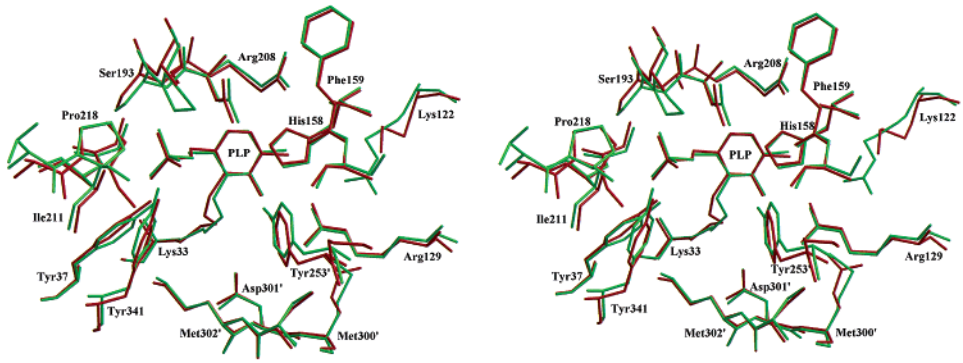

FIGURE 6: Stereoview of the superposition of the active site residues of DadX (green) and Alr (red) obtained after a least-squares fit of the C_α atoms of their N-terminal domains. The residue numbers are those from the DadX structure.

differences in strand grouping and the shorter C-terminus of DadX.

Structural Comparison of the Active Sites. The geometry of the active site, which is comprised of residues from both monomers, is strongly conserved between DadX and Alr (Figure 6). This is the case despite the difference in the interdomain rotation between these two species. The rms difference for the C_α atoms of these residues, namely, 27−34, 53−58, 73−79, 95−99, 117−132, 152−166, 187−194, and 205−210 (DadX numbers) is 0.86 Å. There is clear contiguous electron density between Lys33 and the C4′ atom of PLP, consistent with a covalent internal aldimine linkage.

Strong Extra Density in the Active Site. Perhaps the most striking features of the DadX active site is an electron density cluster near the face of PLP, exactly in the region where acetate (*20*) and propionate (*21*) are located in the *Bacillus* structures (Figure 7). Its shape resembles that of a four to five atom long hydrocarbon chain terminated by a bulkier fragment reminiscent of a chiral atom and a carboxylate group (Figure 7a). As discussed in the Materials and Methods, following attempts to interpret this density as solvent, buffer, and precipitant molecules, we found that the best geometrical fit was obtained with a molecule of D-lysine oriented such that its terminal nitrogen atom NZ points toward the PLP cofactor. Furthermore, $2F_{obs} - F_{calc}$ density from the C4′ position of PLP protrudes toward the density of this guest compound and contacts it at a distance that indicates the possibility of a fractionally occupied covalent bond.

To test our assumption, refinement was performed assuming (i) D-lysine as the model for the additional electron density in the DadX active site, (ii) two PLP orientations with partial occupancy, and (iii) D-lysine tethered to PLP through a second aldimine bond. Following refinement, the *R*-factors remained basically unchanged, but the *B*-factor for the C4′ position forming the internal aldimine decreased from 23.1 to 14.9 Å^2. The average *B*-factor for the pyridine ring was very similar for both PLP orientations at 14.9 and 14.4 Å^2, respectively. The *B*-factor for the C4′ position linked to the putative substrate refined to 28.8 Å^2, and those for the atoms of D-lysine averaged 42.8 Å^2. As can be seen in Figure 7b, the Fourier difference maps obtained after refinement show acceptable electron density for the central portion of the guest substrate but mediocre electron density for the terminal side-chain atoms. Other attempts to build and interpret this extra electron density as described in the

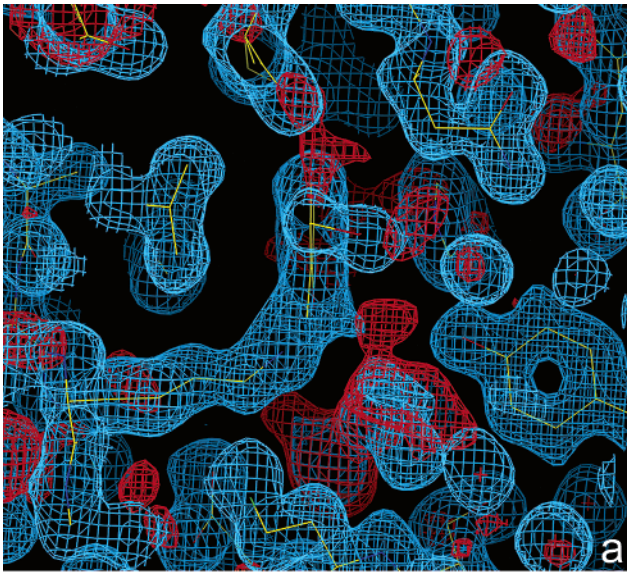

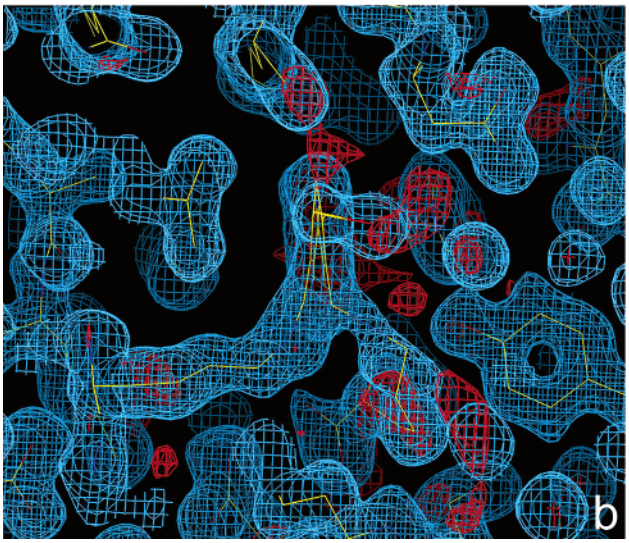

FIGURE 7: $2F_{obs} - F_{calc}$ (blue, contoured at 1.3σ) and $F_{obs} - F_{calc}$ (red, contoured at 1.7σ) electron density maps in the active site of DadX obtained (a) before modeling the electron density of the guest substrate and (b) after modeling the guest substrate with D-lysine and allowing the PLP to adopt two alternate positions with partial occupancy.

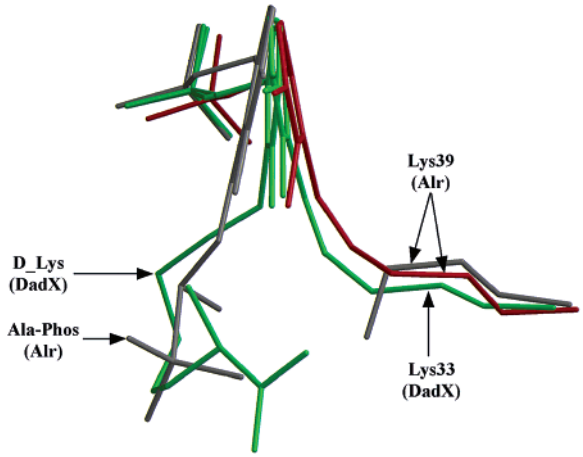

FIGURE 8: Superposition of the PLP cofactors from the DadX (green), Alr/acetate (red), and Alr/alanine phosphonate (gray) structures obtained after a least-squares fit.

Materials and Methods were less successful, including refining this region as a cluster of three solvent molecules. None of the alternatives we tried was completely satisfactory. While recognizing the speculative nature of our attempt to account for this density, we believe the best choice at present is to interpret this density as a partially ordered guest molecule, possibly a D-lysine, that may be covalently interacting with PLP.

Orientation and Binding of PLP. In the active site of DadX, two PLP molecules are located with an angular displacement between them of about 12°. One maintains an internal aldimine linkage with the protein, while the second maintains an external aldimine linkage with the guest substrate. The two orientations are reminiscent to those observed in the internal (*20*, *21*) and external (*22*) complexes of Alr from *Bacillus* (Figure 8). The internal aldimine nitrogen forms a hydrogen bond with O3′ of the internal PLP (2.94 Å), consistent with the protonated nature of the internal Schiff base. Note that, without the imposition of any planarity restraints, the NZ of Lys33 is almost exactly in the plane of the PLP to which it is bound.

In the complex of alanine phosphonate with Alr (*22*), the imine-PLP-phenol system is planar, and a hydrogen bond is observed between the external imine nitrogen and the O3′ of PLP. This geometry is consistent with mechanisms that propose electron delocalization into the PLP ring during formation of the carbanion intermediate, a process thought to occur during catalysis by alanine racemase (*20*) and by other PLP-dependent enzymes (*37*−*39*). However, the electron density for the external aldimine in our structure is not clear enough to allow for an unambiguous determination of its geometry relative to PLP.

Since both the internal and the external aldimine forms appear to be present in the DadX structure, two explanations are readily apparent. It may be that a statistical mix of internal and external aldimine forms is present in the active sites. If this were the case, we would expect to see evidence of two states for Lys33, one linked to PLP and one not involved in the aldimine linkage. These two states have been reported in the internal and external complexes of *Bacillus* Alr, for example. However, in the DadX structure, the *B*-factor for the terminal NZ of Lys33 is 19.8 Å^2, and there is no sign of any alternate conformation for Lys33. A second explanation for our results is that the PLP is involved in a dynamic equilibrium in which both internal and external aldimine forms interchange continuously (Scheme 1). The electron density and *B*-factor values for the active site atoms are more consistent with this hypothesis.

Hydrogen Bonding with PLP. The hydrogen bond network in the active site of DadX involving PLP, substrate, and nearby residues, as illustrated in Figures 9 and 10, is very similar to that of Alr. One important feature found in both structures is a strong hydrogen bond between the nitrogen atom N1 of the pyridine ring of PLP and the nitrogen atom NE of the nearby positively charged arginine. In Alr, the distance ranges from 2.6 to 2.9 Å, while it is 2.8 Å in DadX. In most other PLP enzymes, the N1 atom of PLP interacts with a negatively charged carboxylate, consistent with its protonated nature (*37*). For alanine racemase, some structural reports have referred to N1 as being protonated (*20*, *26*), while others at times have depicted N1 as being unprotonated

Scheme 1

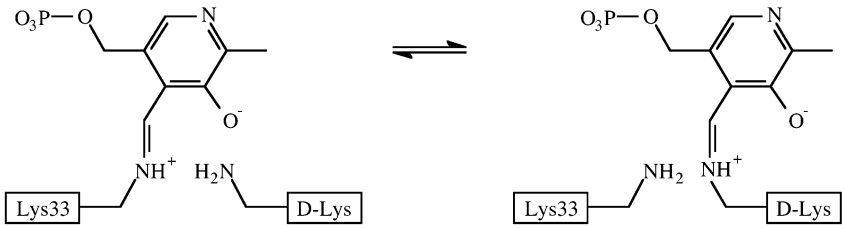

(*21*, *22*). Mechanistic schemes that accommodate either protonation state have been reported (*40*, *41*).

We believe in DadX the close interaction between N1 and a positively charged arginine is more consistent with N1 remaining unprotonated. This interaction would still allow for stabilization of the postulated carbanion intermediate through electron delocalization into the ring. In addition, we note that His158 in DadX partially overlaps and is 3.4 Å away from the PLP ring. Poisson−Boltzmann calculations indicate that this histidine is protonated at neutral pH. This nearby histidine might also help stabilize the PLP during racemization of alanine possibly through $\pi-\pi$ and/or charge-transfer interactions with the histidine ring (*42*, *43*) (Figure 10).

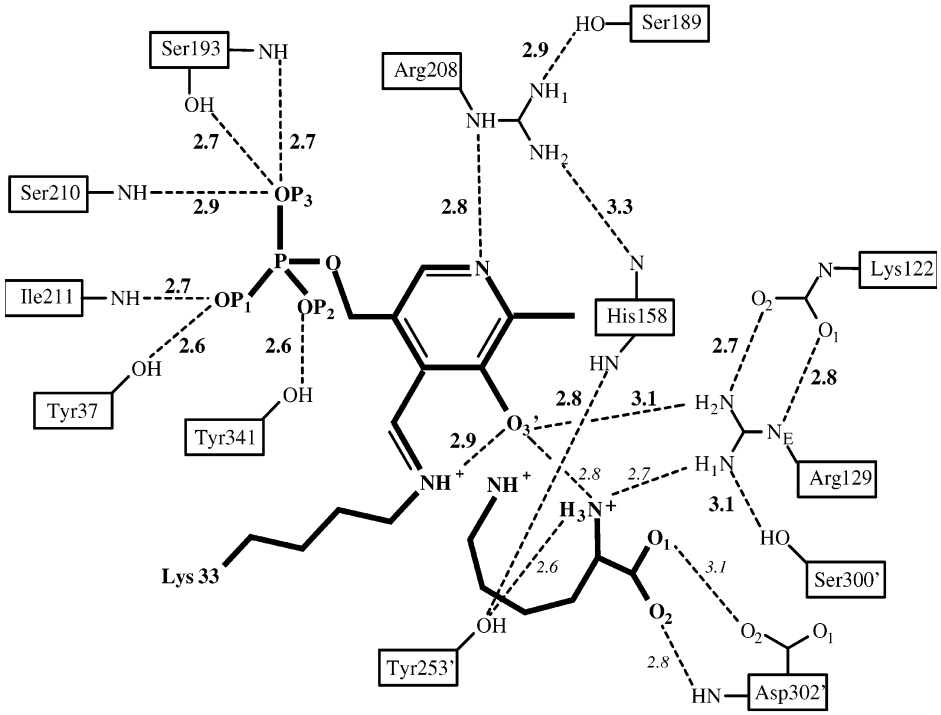

FIGURE 9: Schematic diagram of the hydrogen bond and salt bridge network in the active site of DadX. For clarity purposes, only the PLP linked to Lys33 has been represented. Bold distances are derived from a model containing one PLP cofactor (see Figure 7a). Distances in italics are derived from a model containing two partially occupied PLP molecules and the guest substrate, D-Lys. Residues from the second monomer are identified with primed numbers.

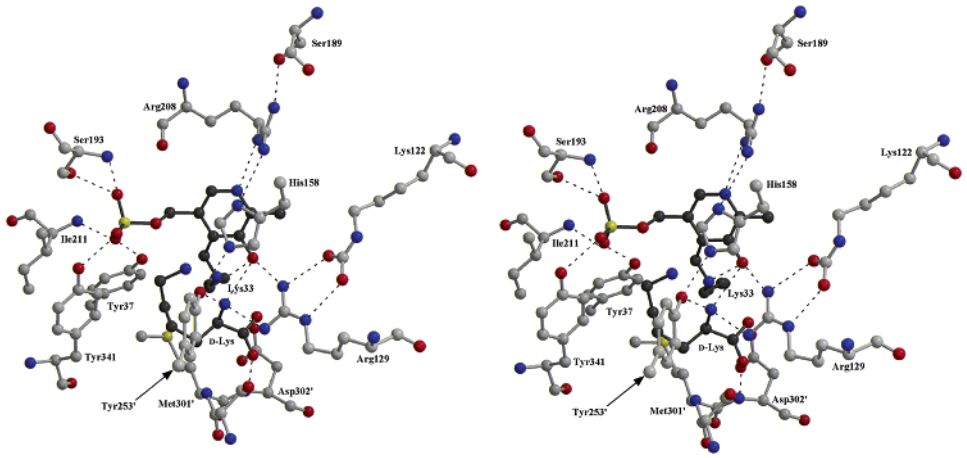

FIGURE 10: Stereoview of the hydrogen bond and salt bridge network in the active site of DadX. For clarity purposes, the second PLP cofactor involved in the interaction with the guest substrate has been omitted.

Within the DadX active site, Arg208 is stabilized by a hydrogen bond network similar to that found in Alr and includes Tyr253′, His158, Arg208, and Ser189. Ser189 replaces His200 of Alr and makes hydrogen contact with only one residue (Arg208), while His200 in Alr communicates with two other histidines (His166 and His127). Consequently, this network in DadX is shortened by two residues. The phenolic oxygen O3′ of PLP in DadX is part of a hydrogen bond network that is essentially identical to that found in Alr, in which O3′ forms a hydrogen bond with Arg129 in DadX and Arg136 in Alr.

As was reported for the Alr/proprionate structure, we observe extra electron density consistent with a carbamylated lysine at the NZ terminus of Lys122 (Lys129 in Alr). Lys122 refines successfully as a carbamylated residue and in its final position forms two hydrogen bonds with Arg129. This suggests that a carbamylated lysine may be a conserved feature of alanine racemase and supports the hypothesis of Ringe that this lysine helps to position the nearby arginine for an interaction with both PLP and substrate.

Entryway to the Binding Pocket. The entrance to the active site of DadX is a corridor defined by OD2 of Asp163, CG2 of Ile339, NH2 of Arg278′, and the main chain nitrogen of Gly254′. This entry corridor is about 11.0 Å long and directly leads to the reactive atom C4′ of PLP. At its end, it is delimited by two tyrosines, Tyr341 and Tyr253′. These residues define an opening with a width of about 2.7 Å. This opening is too narrow for a carbon atom to penetrate (van der Waals radius of 3.4 Å) but is similar to that measured between the corresponding tyrosine residues in the active site of the *Bacillus* structures (ca. 3.0 Å). This suggests that one or both tyrosines must move to allow small substrates to enter and that the entry of larger molecules may be blocked. Studies of alanine racemase in which one of these tyrosines is mutated to alanine confirm that access to the active site is significantly improved (*44*). Teleologically, it makes sense for alanine racemase to severely restrict active site access, thereby avoiding indiscriminant and potentially dangerous amino acid racemization.

Binding Pocket. Substrates that successfully progress past the entry corridor enter a binding cavity of about 5.0 by 3.0 by 3 Å adjacent to the PLP cofactor. Acetate, propionate, alanine phosphonate, and the putative substrate in DadX are all located in this region in the structures of complexes reported to date (*20*−*22*). This cavity is delimited on one side by PLP, the side chain of Met301′, and the side chains of Tyr37 and Tyr341 (Figure 10). From this initial active site cavity, a second cavity on the opposite side of PLP is accessible. This cavity is of a dimension 6.0 by 4.5 by 7.5 Å and contains four water molecules in all *Bacillus* structures. The boundary of this pocket is formed by residues Lys33, Ala58, Leu78, Glu79, carb-Lys122, Arg129, Val130, Asp302′, and Met303′. One of the four waters (Wat 765 in Alr) is replaced in DadX by the carboxylate group of the D-lysine, suggesting that this second cavity can participate in substrate binding. The three remaining waters occupying this cavity are located in the same positions in the Alr complexes with acetate, propionate, phosphonate, and as reported here, in DadX, suggesting that they may be a conserved feature of the enzyme.

Conclusion and Structural Implications for Drug Design. Alanine racemase has often been proposed as a target for drug design in antimicrobial development, given its biological position of being essential to prokaryotes but essentially absent from eukaryotes. Inspection of the structure suggests that there are at least three ways to design inhibitors to the enzyme. One way would be to place an inhibitor within the active site. A second way would be to block access to the active site by placing an inhibitor within the entryway. A third method would be to design an inhibitor that would prevent dimerization. The first method is the most straightforward, but Alr has the reputation of possessing a small active site pocket that would not readily allow for successful drug design. Inspection of our structure reveals that the active site pocket is large enough to accommodate drug candidates. Also, this active site contains several excellent candidates for hydrogen bonding as well as hydrophobic interaction. In fact, compounds up to molecular weight 350 have been computationally docked and clustered (*45*). However, based on analysis of this and earlier alanine racemase structures, a problem does exist with regard to the size of the entryway. In fact, the static DadX structure would not even admit alanine itself into the binding cavity. However, certainly alanine and other molecules do enter the active site, albeit with difficulties commensurate with their size, but this issue has to be taken into account when designing inhibitors. Adopting the second approach would involve the design of compounds to block the entryway. This would avoid the problem of access to the active site but would be more difficult in terms of pharmacophore development. Dimerization inhibitors of alanine racemase have not yet been developed, but the concept has been demonstrated (*46*−*48*). We believe that attempts to design inhibitors using any of these approaches is warranted and of potentially significant biomedical importance. Continued crystallographic study of these enzymes and their complexes with inhibitors will also be of help in these ongoing drug design efforts.

ACKNOWLEDGMENT

Use of the Advanced Photon Source was supported by the U.S. Department of Energy, Basic Energy Sciences, Office of Science, under Contract W-31-109-Eng-38. Use of the BioCARS Sector 14 was supported by the National Institutes of Health, National Center for Research Resources, under Grant RR07707. We thank Profs. James Briggs and Harold Kohn and Drs. Chetlen Crossnoe and Gabriela Mustata for helpful comments and discussions. We also thank the Institute of Molecular Design and Molecular Simulations, Inc. for the use of computational resources.

REFERENCES

1. Pollack, M. (1995) *Pseudomonas aeruginosa*, in *Principles and Practice of Infectious Diseases* (Mandell, G. L., Bennett, J. E., and Dolin, R., Eds.) pp 2310−2335, Churchill Livingstone, New York.
2. Martone, W. J., and Jarvis, W. R. (1992) Predominant Pathogens in Hospital Infections, *J. Antimicrob. Chemother.* 19−24.
3. FitzSimmons, S. C. (1993) The Changing Epidemiology of Cystic Fibrosis, *J. Pediatr.* 1−9.
4. Bert, F., Maubec, E., and Bruneau, B. et al. (1998) Multi-resistant *Pseudomonas aeruginosa* Outbreak Associated with Contaminated Tap Water in a Neurosurgery Intensive Care Unit, *J. Hops. Infect.* 53−62.

5. Chen, H. Y., Yuan, M., Ibrahim-Elmagboul, I. B., and Livermore, D. M. (1995) National Survey of Susceptibility to Antimicrobials amongst Clinical Isolates of *Pseudomonas aeruginosa*, *J. Antimicrob. Chemother.* 521−534.
6. Strych, U., Huang, H. C., Krause, K. L., and Benedik, M. J. (2000) Characterization of the Alanine Racemases from *Pseudomonas aeruginosa* PAO1, *Curr. Microbiol. 41*, 290−294.
7. Wasserman, S. A., Walsh, C. T., and Botstein, D. (1983) Two Alanine Racemase Genes in *Salmonella typhimurium* that Differ in Structure and Function, *J. Bacteriol. 153*, 1439−1450.
8. Wild, J., Hennig, J., Lobocka, M., Walczak, W., and Klopotowski, T. (1985) Identification of the *dadx* Gene Coding for the Predominant Isozyme of Alanine Racemase in *Escherichia coli* K12, *Mol. Gen. Genet. 198*, 315−322.
9. Lambert, M. P., and Neuhaus, M. P. (1972) Mechanism of D-Cycloserine Action: Alanine Racemase from *Escherichia coli*, *J. Bacteriol. 110*, 978−987.
10. Silverman, R. B. (1988) The Potential Use of Mechanism-Based Enzyme Inactivators in Medicine, *J. Enzyme Inhib. 2*, 73−90.
11. Copie, V., Faraci, W. S., Walsh, C. T., and Griffin, R. G. (1988) Inhibition of Alanine Racemase by Alanine Phosphonate: Detection of an Imine Linkage to Pyridoxal 5′-Phosphate in the Enzyme Inhibitor Complex by Solid-State ^{15}N Nuclear Magnetic Resonance, *Biochemistry 27*, 4966−4970.
12. Erion, M. D., and Walsh, C. T. (1987) 1-Aminocyclopropanephosphonate: Time-Dependent Inactivation of 1-Aminocyclopropanecarboxylate Deaminase and *Bacillus stearothermophilus* Alanine Racemase by Slow dissociation Behavior, *Biochemistry 26*, 3417−3425.
13. Wang, E., and Walsh, C. T. (1978) Suicide Substrates for the Alanine Racemase from *Escherichia coli B*, *Biochemistry 17*, 1313−1321.
14. Neuhaus, F. C. (1967) Mechanism of Action, in *Antibiotics* (Gottleib, D., and Shaw, P. D., Eds.) pp 40, Springer-Verlag, New York.
15. Walsh, C. (2003) Antibiotics that Act on Cell Wall Biosynthesis, in *Antibiotics—actions, origins, resistance*, pp 23−49, ASM Press, Washington.
16. Weinstein, L. (1975) Antimicrobial Agents—Drugs Used in the Chemotherapy of Tuberculosis and Leprosy, in *The Pharmacological Basis of Therapeutics, 5th ed.* (Goodman, L. S. and Gilman, A., Eds.) pp 1202−1223, Macmillan Publishing, New York.
17. Newton, R. W. (1975) Side Effects of Drugs Used to Treat Tuberculosis, *Scott. Med. J. 20*, 47−49.
18. Yew, W. W., Wong, C. F., Wong, P. C., Lee, J., and Chau, C. H. (1993) Adverse Neurological Reactions in Patients with Multidrug-Resistant Pulmonary Tuberculosis after Coadministration of Cycloserine and Ofloxacin, *Clin. Infect. Dis. 17*, 288−289.
19. Katz, M. H. (1994) Effect of HIV Treatment on Cognition, Behavior, and Emotion, *Psychiatr. Clin. North Am. 17*, 227−230.
20. Shaw, J. P., Petsko, G. A., and Ringe, D. (1997) Determination of the Structure of Alanine Racemase from *Bacillus stearothermophilus* at 1.9 Å Resolution, *Biochemistry 36*, 1329−1342.
21. Morollo, A. A., Petsko, G. A., and Ringe, D. (1999) Structure of a Michaelis Complex Analogue: Propionate Binds in the Substrate Carboxylate Site of Alanine Racemase, *Biochemistry 38*, 3293−3301.
22. Stamper, C. G. F., Morollo, A. A., and Ringe D. (1998) Reaction of Alanine Racemase with 1-Aminoethylphosphonic Acid Forms a Stable External Aldimine, *Biochemistry 37*, 10438−10445.
23. Jansonius, J. N. (1998) Structure, Evolution and Action of Vitamin B(6) Dependent Enzymes, *Curr. Opin. Struct. Biol. 8*, 756−759.
24. Ondrechen, M. J., Briggs, J. M., and McCammon, J. A. (2001) A Model for Enzyme−Substrate Interaction in Alanine Racemase, *J. Am. Chem. Soc. 123*, 2830−2834.
25. Watanabe, A., Yoshimura, T., Mikami, B., and Esaki, N. (1999) Tyrosine 265 of Alanine Racemase Serves as a Base Abstracting a Hydrogen from L-Alanine: the Counterpart Residue to Lys39 Specific to D-Alanine, *J. Biochem. 126*, 781−786.
26. Fenn, T. D., Stamper, G. F., Morollo, A. A., and Ringe, D. (2003) A side Reaction of Alanine Racemase: Transamination of Cycloserine, *Biochemistry 42*, 5775−5783.
27. Olson, G. T., Mengmeng, F., Lau, S., Rinehart, K. L., and Silverman, R. B. (1998) An Aromatization Mechanism of Inactivation of γ-Aminobutyric Acid Aminotransferase for the Antibiotic L-Cycloserine, *J. Am. Chem. Soc. 120*, 2256−2267.
28. Peisach, D., Chipman, D. M., Van Ophem, P. W., Manning, J. M., and Ringe, D. (1998) D-Cycloserine Inactivation of D-Amino Acid Aminotransferase Leads to a Stable Noncovalent Protein Complex with an Aromatic Cycloserine-PLP Derivative, *J. Am. Chem. Soc. 120*, 2268−2274.
29. Yokoigawa, K., Okubo, Y., and Soda, K. (2003) Subunit Interaction of Monomeric Alanine Racemases from Four *Shigella* Species in Catalytic Reaction, *FEMS Microbiol. Lett. 221*, 263−267.
30. Otwinowski, Z., and Minor, W. (1997) Processing of X-ray Diffraction Data Collected in Oscillation Mode, in *Methods of Enzymology* (C. W. Carter, J., and Sweet, R. M., Eds.) pp 307−326, Academic Press, New York.
31. Terwilliger, T. C., and Berendzen, J. (1999) Automated Structure Solution for MIR and MAD, *Acta Crystallogr. D55*, 849−861.
32. Lamzin, V. S., and Wilson, K. S. (1997) Automated Refinement for Protein Crystallography, *Methods Enzymol. 277*, 269−305.
33. Perrakis, A., Sixma, T. K., Wilson, K. S., and Lamzin, V. S. (1997) wARP: Improvement and Extension of Crystallographic Phases by Weighted Averaging of Multiple Refined Dummy Atomic Models, *Acta Crystallogr. D53*, 448−455.
34. Perrakis, A., Morris, R. J., and Lamzin, V. S. (1999) Automated Protein Model Building Combined with Iterative Structure Refinement, *Nat. Struct. Biol. 6*, 458−463.
35. Sheldrick, G. M., and Schneider, T. R. (1997) Shelxl: High-Resolution Refinement, *Methods Enzymol. 277*, 319−343.
36. Jones, T. A., Zou, J. Y., Cowan, S. W., and Kjeldgaard, M. (1991) Improved Methods for Building Protein Models in Electron Density Maps and the Location of Errors in these Models, *Acta Crystallogr. A47*, 110−119.
37. Yano, T., Kuramiysu, S., Tanase, S., Morino, Y., and Kagamiyama, H. (1992) Role of Asp222 in the Catalytic Mechanism of *Escherichia coli* Aspartate Aminotransferase: The Amino Acid Residue Which Enhances the Function of the Enzyme-Bound Coenzyme Pyridoxal 5′-Phosphate, *Biochemistry 31*, 5878−5887.
38. Arnone, A., Christen, P., Jansonius, J. N., and Metzler, D. E. (1985) in *Transaminases* (Christen, P., and Metzler, D. E., Eds.) pp 326−357, John Wiley and Sons, New York.
39. McPhalen, C. A., Vincent, M. G., and Jansonius, J. N. (1992) X-ray Structure Refinement and Comparison of Three Forms of Mitochondrial Aspartate Aminotransferase, *J. Mol. Biol. 225*, 495−517.
40. Ashley Spies, M., and Toney, M. D. (2003) Multiple Hydrogen Kinetic Isotope for Enzymes Catalyzing Exchange with Solvent: Application to Alanine Racemase, *Biochemistry 42*, 5099−5107.
41. Watanabe, A., Yoshimura, T., Mikami, B., Kagamiyama, H., and Esaki, N. (2002) Reaction Machanism of Alanine Racemase from *Bacillus stearothermophilus*, *J. Biol. Chem. 277*, 19166−19172.
42. Rathore, R., Lindeman, S. V., and Kochi, J. K. (1997) Charge-Transfer Probes for Molecular Recognition via Steric Hindrance in Donor−Acceptor Pairs, *J. Am. Chem. Soc. 119*, 9393−9404.
43. Le Magueres, P., Lindeman, S. V., and Kochi, J. K. (2000) Novel (Heteromolecular) π-Complexes of Aromatic Cation Radicals. Isolation and Structural Characterization, *Org. Lett. 2*, 3567−3570.
44. Wayne, M. P., Weisner, J., and Blackburn, J. M. (2002) Site-Directed Mutagenesis of Tyr354 in *Geobacillus stearothermophilus* Alanine Racemase Identifies a Role in Controlling Substrate Specificity and a Possible Role in the Evolution of Antibiotic Resistance, *ChemBioChem 8*, 789−792.
45. Mustata, G. I., and Briggs, J. M. (2002) A Structure-Based Design Approach for the Identification of Novel Inhibitors: Application to an Alanine Racemase, *J. Comput.-Aided Mol. Des. 16*, 935−953.
46. Boggetto, N., and Reboud-Ravaux, M. (2002) Dimeric Inhibitors of HIV-1 Protease, *Biol. Chem. 383*, 1321−1324.
47. Song, M., Rajesh, S., Hayashi, Y., and Kiso, Y. (2001) Design and Synthesis of New Inhibitors of HIV-1 Protease Dimerization with Conformationally Constrained Templates, *Bioorg. Med. Chem. Lett. 11*, 2465−2468.
48. Cochran, A. G. (2001) Protein−Protein Interfaces: Mimics and Inhibitors, *Curr. Opin. Chem. Biol. 5*, 654−659.

BI030165V